BIOPHYSICS

Functional protein dynamics on uncharted time scales detected by nanoparticle-assisted NMR spin relaxation

Mouzhe Xie[1]*, Lei Yu[1]*, Lei Bruschweiler-Li[2], Xinyao Xiang[1], Alexandar L. Hansen[2], Rafael Brüschweiler[1,2,3]†

Protein function depends critically on intrinsic internal dynamics, which is manifested in distinct ways, such as loop motions that regulate protein recognition and catalysis. Under physiological conditions, dynamic processes occur on a wide range of time scales from subpicoseconds to seconds. Commonly used NMR spin relaxation in solution provides valuable information on very fast and slow motions but is insensitive to the intermediate nanosecond to microsecond range that exceeds the protein tumbling correlation time. Presently, very little is known about the nature and functional role of these motions. It is demonstrated here how transverse spin relaxation becomes exquisitely sensitive to these motions at atomic resolution when studying proteins in the presence of nanoparticles. Application of this novel cross-disciplinary approach reveals large-scale dynamics of loops involved in functionally critical protein-protein interactions and protein-calcium ion recognition that were previously unobservable.

INTRODUCTION

Nuclear magnetic resonance (NMR) spin relaxation measurements of proteins offer a wealth of information at atomic resolution about internal motional amplitudes and time scales under physiological conditions (*1*–*4*). This dynamics information provides critical mechanistic and thermodynamic insights into protein function involving loop motions, interdomain dynamics, recognition dynamics with small ligands, nucleic acids or other proteins, and partial unfolding/refolding events (*5*–*13*).

Every type of NMR parameters—such as scalar *J*-couplings, residual dipolar couplings, and average chemical shifts—depends in a unique way on both molecular structure and dynamics (*1*). In the case of spin relaxation parameters, the observable range of intramolecular protein motions covers fast time scales in the picosecond to low nanosecond range via longitudinal spin relaxation R_1, transverse spin relaxation R_2, and the heteronuclear Overhauser enhancement (NOE) experiments (*1*). By contrast, the chemical exchange and conformational exchange regime on tens of microseconds to seconds is covered by rotating frame relaxation experiments [$R_{1\rho}$, Carr-Purcell-Meiboom-Gill (CPMG), and chemical exchange saturation transfer] (*14*–*17*). R_1, R_2, and NOE relaxation data represent the convolution of overall rotational tumbling and intramolecular dynamics, which renders motions unobservable if they take place on time scales slower than the overall tumbling correlation time τ_P, which is typically around 10 ns. Thus, the intermediate time scale regime between low nano- and microsecond motions represents a critical gap in our ability to directly observe protein dynamics. The mere existence and atomic-detail character of these motions and their role in protein function are therefore largely uncharted territory.

As described in the paper, this situation can be addressed by studying protein dynamics in the presence of aqueous colloidal dispersions of synthetic nanoparticles (NPs) (Fig. 1). With their much larger size, NPs have tumbling correlation times $\tau_{NP} >> \tau_P$ into the hundreds of nanosecond to microsecond range (*18*). For proteins that transiently interact with the NP surface and are in rapid exchange between a free and an NP-bound state, their spin relaxation reflects dynamics on the much broader picosecond to τ_{NP} range, thereby offering an unobstructed view of pico- to microsecond motions.

RESULTS

Transverse R_2 spin relaxation experiments (*1*) are particularly sensitive to the presence of NPs. Consider a protein with an overall tumbling correlation time τ_P, which is intermittently bound to an NP with correlation time τ_{NP} with an exchange rate that is fast on the NMR chemical shift time scale ($>10^3$ s^{-1}) but slow on the molecular tumbling time scale ($<10^7$ to 10^8 s^{-1}). The effective transverse relaxation rate of a protein ^{15}N spin is then

$$R_2^{NP} = pR_2^{bound} + (1-p)R_2^{free} \quad (1)$$

where p and $1-p$ are the bound and free protein populations with transverse relaxation rates R_2^{bound} and R_2^{free}, respectively. R_2 is dominated by the spectral density of motion at zero frequency $R_2 = cJ(0)$, where c is a constant (see the Supplementary Materials). When internal dynamics is represented for each ^{15}N site in a model-free way with an S^2 order parameter and an internal correlation time τ_i (*19*), $J^{free}(0) = S^2\tau_P + (1-S^2)\frac{\tau_P\tau_i}{\tau_P+\tau_i}$ and $J^{bound}(0) = S^2\tau_{NP} + (1-S^2)\frac{\tau_{NP}\tau_i}{\tau_{NP}+\tau_i}$, where $\tau_{i,P}^{-1} = \tau_P^{-1} + \tau_i^{-1}$ and $\tau_{i,NP}^{-1} = \tau_{NP}^{-1} + \tau_i^{-1}$ (used below). S^2 is a general measure of the motional restriction of a ^{15}N-^{1}H bond vector varying between 0 (highly mobile) and 1 (static). The difference of R_2 in the presence and absence of NPs, ΔR_2, can then be expressed as

$$\begin{aligned}\Delta R_2/(cp) &= \left(R_2^{NP} - R_2^{free}\right)/(cp) \\ &= S^2(\tau_{NP} - \tau_P) + (1-S^2)(\tau_{i,NP} - \tau_{i,P}) \end{aligned} \quad (2)$$

If $|\tau_{NP} - \tau_P| \gg |\tau_{i,NP} - \tau_{i,P}|$, which applies when $\tau_i < \tau_{NP}/10$ and S^2 is nonzero, then Eq. 2 reduces to

$$S^2 \cong \Delta R_2/(cp\,\tau_{NP}) \quad (3)$$

It follows that the site-specific S^2 order parameters can be directly extracted from experimental ΔR_2 values whereby the global scaling

[1]Department of Chemistry and Biochemistry, The Ohio State University, Columbus, OH 43210, USA. [2]Campus Chemical Instrument Center, The Ohio State University, Columbus, OH 43210, USA. [3]Department of Biological Chemistry and Pharmacology, The Ohio State University, Columbus, OH 43210, USA.
*These authors contributed equally to this work.
†Corresponding author. Email: bruschweiler.1@osu.edu

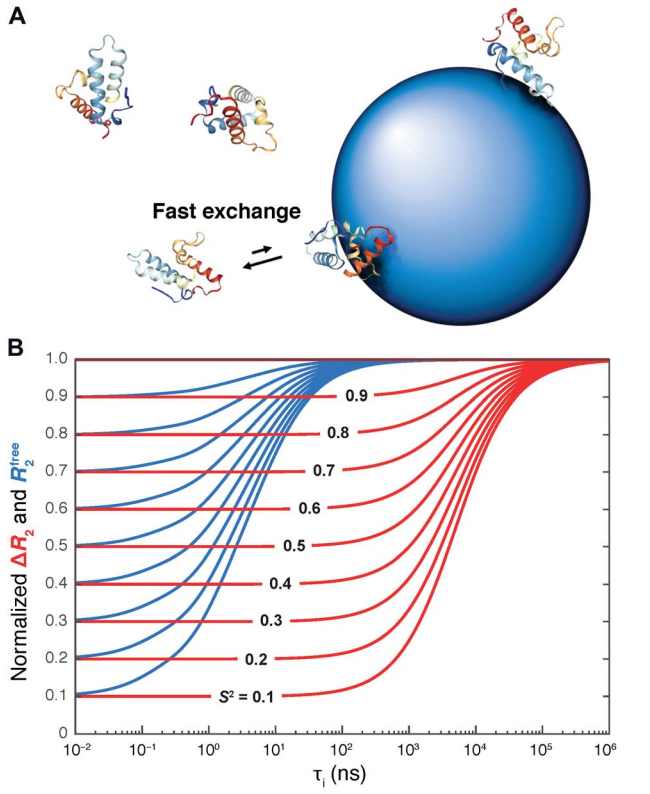

Fig. 1. Protein dynamics into the hundreds of nanosecond to microsecond range accessible to NP-assisted solution NMR. (**A**) Protein molecules are in fast exchange between their rapidly tumbling free state and a slowly tumbling NP-bound state giving rise to effective transverse spin relaxation rates R_2^{NP} versus R_2^{free} in the absence of NPs. (**B**) Simulated dependence of R_2^{free} in the absence of NPs (blue) and $\Delta R_2 = R_2^{NP} - R_2^{free}$ in the presence and absence of NPs (red) on the internal correlation time τ_i and motional restriction (S^2 order parameter), which demonstrates the wide range of time scales sensitively probed by ΔR_2. The blue and red curves were normalized by setting their maximal values to 1.0.

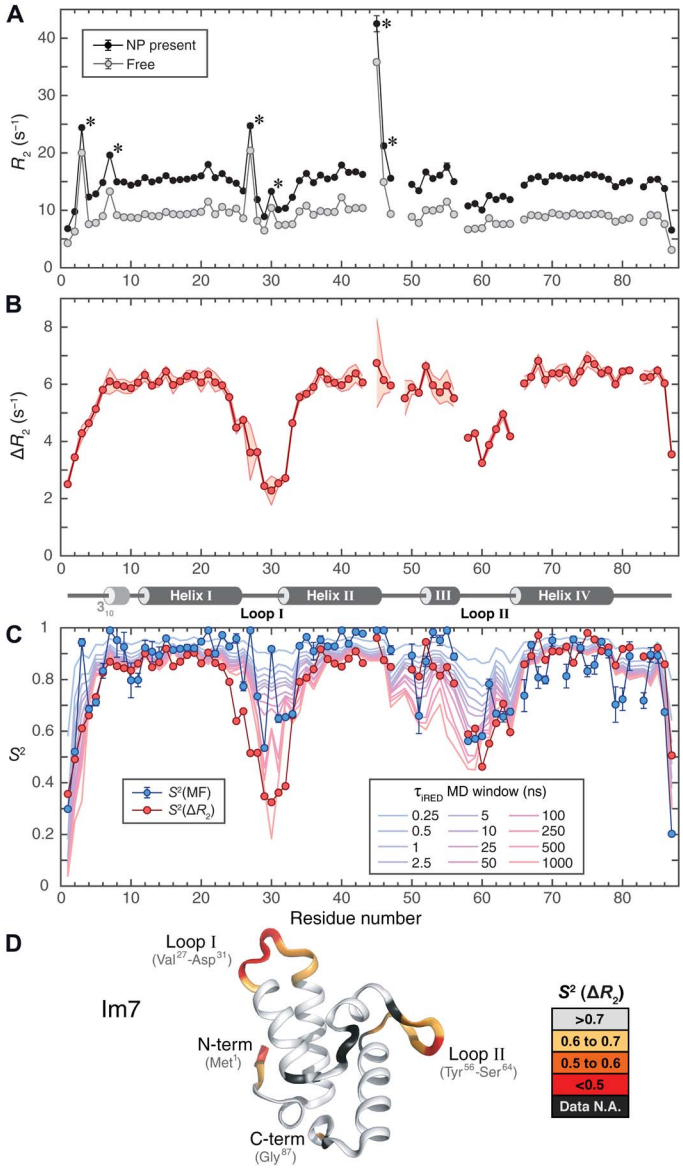

Fig. 2. Dynamics of Im7 protein by backbone ^{15}N-NMR spin relaxation and molecular dynamics (MD) simulations. (**A**) ^{15}N-R_2 relaxation rates measured in the absence (gray) and presence (black) of NPs. Data points with asterisks (*) indicate substantial chemical exchange R_{ex} effects. (**B**) R_2 differences (ΔR_2) of (A) with secondary structure of Im7 indicated at the bottom (4 α helices and 3_{10} helix at N terminus). Experimental uncertainty (1 SD) is depicted by the shaded red area based on five independently measured ΔR_2 profiles (see fig. S6). (**C**) Comparison of ΔR_2-derived S^2 (red circles) with standard model-free S^2 order parameters (blue circles) and S^2 values determined from 1-μs MD trajectory with variable averaging time window (from 250 ps to 1 μs). (**D**) $S^2(\Delta R_2)$ values mapped on three-dimensional (3D) crystal structure [Protein Data Bank (PDB) code 1AYI] show loops and tails that undergo substantial dynamics on pico- to microsecond time scales. N.A., not available.

factor $(c\,p\tau_{NP})^{-1}$ is identical for all residues. Since ΔR_2-derived S^2 reflects the cumulative effect of all internal motions with correlation times $\tau_i < \tau_{NP}/10$, it exceeds the time scale range $\tau_i < \tau_P$ of standard model-free S^2 values determined in the absence of NPs by several orders of magnitude (Fig. 1B). The validity range of Eq. 3 is depicted in fig. S2.

NP-assisted NMR relaxation is demonstrated for the two globular proteins colicin E7 immunity protein (Im7) and calcium-binding domain 1 of the canine sodium-calcium exchanger NCX1 (CBD1). Im7 forms a four-helix bundle and binds to the deoxyribonuclease (DNase) domain of bacteriocin colicin E7 (ColE7), thereby inhibiting its strong toxic effect (*20*). Because Im7 exhibits an on-pathway folding intermediate, it has served as a model system for studying protein folding (*21*, *22*). CBD1 is a globular domain with a β-sandwich fold and is part of the large cytosolic loop of the sodium-calcium exchanger (NCX) (*23*). CBD1, which is studied here in the absence of Ca^{2+}, can bind up to four Ca^{2+} ions that produce an allosteric response that allows the exchange of intracellular Ca^{2+} with extracellular Na^+ ions across the transmembrane domain of NCX (*24*).

Backbone ^{15}N R_2 relaxation parameters were measured in the presence and absence of submicromolar to low micromolar anionic silica NPs (SNPs) of 20 nm diameter (Figs. 2A and 3A) with minimal effect on solvent viscosity (*25*). Because of the transient interactions of the protein molecules with SNPs, their average overall tumbling is slowed down, which explains why R_2 in the presence of SNPs exceeds that of the free state. Several residues display enhanced R_2 relaxation, which is caused by chemical exchange R_{ex} on the millisecond time scale and

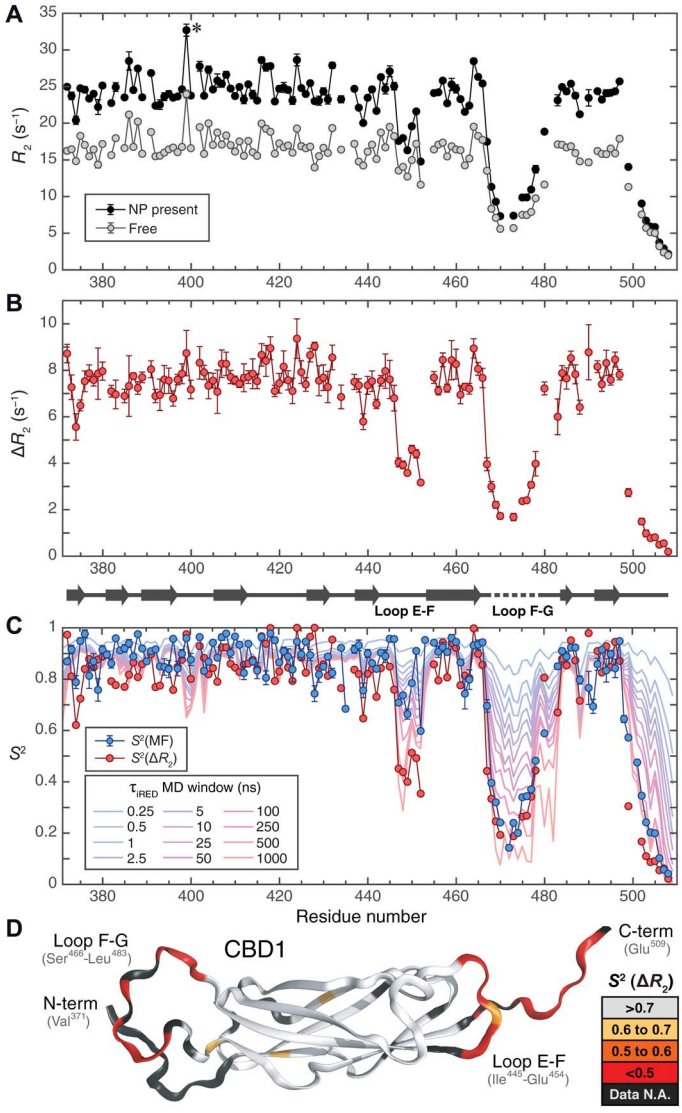

Fig. 3. Dynamics of CBD1 protein domain from backbone ^{15}N-NMR spin relaxation and MD simulations. (**A**) ^{15}N-R_2 relaxation rates measured in the absence (gray) and presence (black) of NPs. Gly^{399} (*) shows substantial chemical exchange R_{ex}. (**B**) R_2 differences (ΔR_2) of (A) with secondary structure of CBD1 indicated at the bottom (nine β strands). (**C**) Comparison of ΔR_2-derived S^2 (red circles) with standard model-free S^2 order parameters (blue circles) and S^2 values determined from 1-μs MD trajectory with variable averaging time window (from 250 ps to 1 μs). (**D**) $S^2(\Delta R_2)$ values mapped on the 3D crystal structure of CBD1 (PDB code 2DPK) show loops and tails that undergo substantial dynamics on pico- to microsecond time scales.

remains largely unaffected by the presence of SNPs. When focusing on ΔR_2 profiles (Fig. 2, B and C), R_{ex} effects cancel out, allowing an interpretation of ΔR_2 solely in terms of S^2 order parameters (Eq. 3). Conformationally rigid regions with large ΔR_2 belong to regular secondary structures and certain loops. At the same time, both proteins show large amounts of dynamics in the N- and/or C-terminal tails and in selected loop regions, manifested in a substantial decrease of their ΔR_2 values. To obtain a quantitative measure of the dynamics, ΔR_2 values were converted to $S^2(\Delta R_2)$ order parameters (Eq. 3) by global scaling so that rigid secondary structures have average $S^2(\Delta R_2)$ values of 0.85 (see the Supplementary Materials). This allows a direct comparison with traditional model-free S^2(MF) values (blue circles in Figs. 2C and 3C) (*22*, *26*) derived from standard ^{15}N R_1, R_2, and NOE data of free protein reporting on picosecond to low nanosecond motions only.

For Loop II of Im7, the $S^2(\Delta R_2)$ and S^2(MF) profiles reflect a very similar degree of mobility with minima around 0.5, which indicates that relevant loop conformations are mostly explored on the fast picosecond to low nanosecond time scale. By contrast, Loop I has $S^2(\Delta R_2)$ values that are substantially lower than S^2(MF), revealing the presence of fast dynamics with S^2(MF) > 0.53 and additional slower motions on the nano- to microsecond range with $S^2(\Delta R_2)$ between 0.32 and 0.53. The $S^2(\Delta R_2)$ profile for Loop I is wider than the S^2(MF) profile and reaches into the C terminus of Helix I (residues Lys^{24}-Val^{27}). This fraying of Helix I is consistent with submicrosecond folding and unfolding of the last helical turn observed in the molecular dynamics (MD) simulation (Fig. 2C). These nano- to microsecond motions were missed in previous studies based on spin relaxation data in the absence of SNPs. Further fraying and partial unfolding occur in a lowly populated folding intermediate, where the stabilizing Glu^{21}-Lys^{24} salt bridge is absent and Glu^{25} exhibits random-coil behavior (*27*).

CBD1 has a total of eight loops connecting the nine β strands (strands A to G). Loop F-G, which is missing in the x-ray crystal structure [Protein Data Bank (PDB) code 2DPK], is most flexible with $S^2(\Delta R_2)$ values <0.2 that are in excellent agreement with the corresponding S^2(MF) values. It suggests that this loop is highly dynamic with dominant correlation times on the pico- to nanosecond time scale that are fully reflected by spin relaxation data both in the presence and absence of SNPs. Loop E-F, which is located at the other end of the protein (Fig. 3D), has a distinctly different behavior. According to standard ^{15}N-relaxation analysis, it is only moderately flexible with S^2(MF) > 0.60. However, $S^2(\Delta R_2)$ values dip as low as 0.35, reflecting the presence of substantial amounts of additional dynamics into the hundreds of nanosecond range. Loop E-F therefore probes a much broader ensemble of conformations than suggested by traditional ^{15}N-relaxation data alone. Similarly, the C-terminal residues of CBD1 also exhibit $S^2(\Delta R_2) < S^2$(MF) caused by dynamics on both the pico- to nanosecond and nano- to microsecond time scales.

Independent corroborating evidence of the presence and location of fast and slow time scale dynamics can be gleaned from extended MD computer simulations. MD trajectories in explicit water solvent were computed and analyzed for both protein systems. ^{1}H-^{15}N S^2 (MD) values, computed from MD trajectories using 12 different isotropic reorientational eigenmode dynamics (iRED) (*28*) time-averaging windows τ_{iRED} ranging from 250 ps to 1 μs, are plotted in Figs. 2C and 3C. Loops I and II in Im7 and Loops E-F and F-G in CBD1 all show a steady drop of S^2(MD) when averaging over slower time scales (longer τ_{iRED} windows), whereas secondary structures and other loops remain notably rigid. Adequate sampling of Loop I conformations is only achieved when considering the full-length trajectory, whereas Loop II samples most of the relevant conformations already within τ_{iRED} ~25 ns, which corresponds to the time scale window accessible by ^{15}N spin relaxation of the free protein (*28*). Similarly, for Loop E-F and the C terminus, the entire 1-μs trajectory length is required to reach good agreement with experimental $S^2(\Delta R_2)$, supporting the experimental finding that this loop displays large amplitude motions on time scales inaccessible by standard NMR relaxation methods.

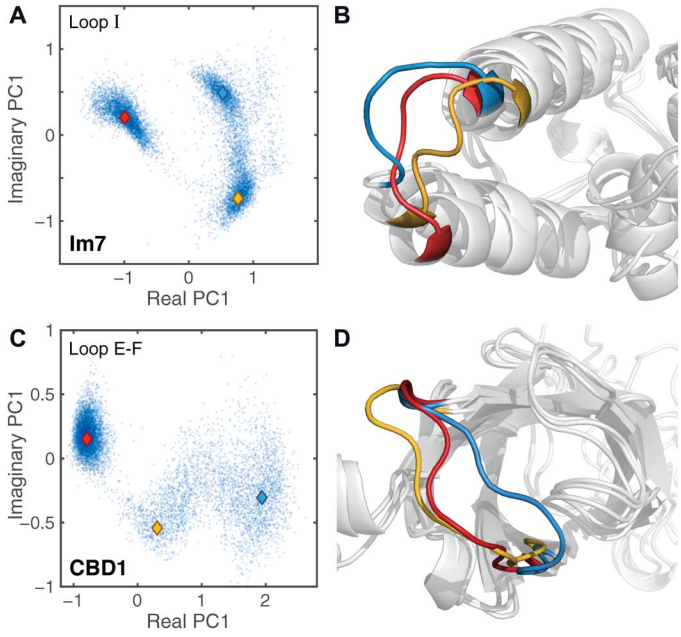

Fig. 4. Visualization of complex loop motions by 1-μs MD trajectories. (**A** and **C**) Backbone dihedral angle–based PCA score plots of (A) Loop I of Im7 and (C) Loop E-F of CBD1 display multiple distinct conformational loop clusters. (**B** and **D**) 3D visualization of three cluster centers for each protein indicated by colored diamond (♦) symbols in score plots.

The fast and slow dynamics of Im7 Loop I and CBD1 Loop E-F were further analyzed by principal component analysis (PCA) in backbone dihedral angle space (*29*). The score plots of Fig. 4 (A and C) show that both loops transition between multiple conformational clusters with representative cluster snapshots depicted in Fig. 4 (B and D). The diverse nature of the conformational loop ensembles reveals multiple possible interaction modes with partner molecules.

DISCUSSION

Despite their potential significance for biological function, observation of internal protein motions on the nano- to microsecond range has been a major challenge in the past. To make this motional regime accessible, rotational tumbling is sometimes slowed down by increasing solvent viscosity through the addition of ethylene glycol or glycerol. However, this also tends to stiffen or slow down internal motions, keeping slower motions mostly out of range of NMR relaxation experiments (*30*, *31*). Alternatively, increasing the size of the molecule, as was shown for RNA, can slow down tumbling and open up observation of slower nanosecond motions (*13*). A recent NMR relaxometry approach, measuring R_1 over a wide range of magnetic field strengths (0.33 to 22.3 T), could access internal protein motions into the low nanosecond range (*32*).

As demonstrated here, the use of slowly tumbling NPs to which a biomolecule can bind in fast exchange offers a general solution to this long-standing challenge. Rapid exchange has been observed in NMR-based NP binding studies of globular (*33*) and intrinsically disordered proteins (*34*). The binding equilibrium between NPs and proteins can be shifted by adjusting the NP concentration in the submicromolar to low micromolar range to optimize NMR line broadening ($\Delta R_2 < 10\ s^{-1}$ with $p \approx 0.01$), allowing ΔR_2 measurements with high accuracy.

For both CBD1 and Im7, NP-assisted spin relaxation reveals previously unknown slow time scale dynamics of loops displaying low $S^2(\Delta R_2)$ values that are directly involved in protein function through electrostatic interactions with their binding partners. Im7 has pico- to femtomolar affinity to its target colicin protein partner (*35*), whereby acidic residues Asp^{31} and Asp^{35} of Im7 Loop I form strong salt bridges with basic colicin residues Arg^{520}, Lys^{525}, and Lys^{528} (fig. S7). For CBD1, Ca^{2+} ions bind to negatively charged side chains of Asp^{446} and Asp^{447} of Loop E-F, which allosterically triggers the exchange of Ca^{2+} versus Na^+ ions through the transmembrane domain (*24*). The central role of electrostatic interactions in biological complex formation is well established (*36*). The dynamic nature and high plasticity of the interacting loops identified here are likely to help fine-tune these interactions and optimize the affinity and specificity with interacting partner proteins and metal ions.

Low $S^2(\Delta R_2)$ values are reporters of previously unknown contributions to the conformational entropy, analogous to S^2(MF) (*12*, *37*), allowing a more quantitative and complete understanding of the thermodynamics of protein-protein and protein-ligand interactions. As demonstrated here (Figs. 2C and 3C), $S^2(\Delta R_2)$ provide powerful benchmarks for the testing (and potential improvement) of computational models, in particular MD simulation protocols and their underlying force fields. As MD trajectories now routinely extend into the hundreds of nano- to microsecond range, there is a pressing need for experimental benchmarks (*38*) that permit evaluation of these trajectories for which $S^2(\Delta R_2)$ profiles are highly suitable.

Because of their spherical shape, SNPs tumble isotropically along with the proteins bound to them (Fig. 1A), which further simplifies the model-free interpretation of ΔR_2. It assumes that protein-NP interactions do not significantly affect protein structure and dynamics, similar to alignment media used for NMR residual dipolar coupling measurements (*39*, *40*). This should hold when a globular protein interacts with NPs mostly in a nonspecific manner, for example, by making contacts with many different surface sections. Specific binding, for example, to a mobile loop, may systematically alter its mobility in the presence of NPs. By comparing ΔR_2, profiles measured for different types of NPs could help identify these situations. For Im7, few residues (Asn^{79}, Gly^{80}, Gly^{83}, Gln^{86}, and Gly^{87}) display $S^2(\Delta R_2) > S^2$(MF). This modest S^2 inversion may reflect chemical exchange contributions with the SNPs, although no line broadening effects were observed in these regions. Because these residues are neither cationic nor hydrophobic, it is unlikely that these residues are limited in their mobility because of direct interactions with the SNPs.

We used anionic SNPs, but other types of NPs should work similarly well for the proteins studied here and other biomolecules. Anionic SNPs have partially dissociated silanol groups at their surface, which give rise to attractive and repulsive electrostatic interactions with charged protein residues. SNPs can also display hydrophobic interactions that are presumably mediated by siloxane groups at the NP surface, but the details of this interaction mechanism are not fully understood (*41*, *42*).

The cross-disciplinary NP-assisted relaxation method introduced here uncovers previously undetected motions on submicrosecond time scales of protein regions that play key roles in the function of these systems by mediating receptor and ligand interactions. It seems likely that protein motions on these time scales are widespread. NP-assisted spin relaxation enables their comprehensive characterization at atomic resolution and shed new light on biomolecular function.

MATERIALS AND METHODS

The full description of Materials and Methods can be found in the Supplementary Materials. A brief summary is provided here.

Sample preparation

Uniformly ^{15}N-labeled and/or ^{13}C-labeled proteins Im7 and CBD1 were overexpressed in *Escherichia coli* with final NMR concentrations of 500 and 400 μM, respectively. For SNP-containing samples, Bindzil 2040 colloidal SNPs (AkzoNobel) with a 20 nm diameter were dialyzed in pH 7.0 buffers and mixed directly with proteins. All samples were stable over the entire course of the NMR data acquisition.

NMR spectroscopy

NMR experiments were performed on Bruker AVANCE III HD spectrometers operating at 850-MHz ^{1}H frequency (19.97 T) for resonance assignments and relaxation measurements at 298 K (for Im7) and 306 K (for CBD1). ^{15}N spin relaxation rates (R_1 and $R_{1\rho}$) for protein samples both in the absence and presence of SNPs, as well as a $\{^1H\}$-^{15}N steady-state NOE experiment in the absence of SNPs, were measured and analyzed using standard two-dimensional NMR ^{15}N relaxation methods (*43*, *44*).

MD simulations

MD simulations were performed by standard methods using the GROMACS 5.1.2 package (*45*) with initial structures of Im7 and CBD1 built on the basis of crystal structures (PDB codes, 1CEI and 2DPK). AMBER ff99SBnmr1 protein force field (*46*) together with the TIP3P explicit water model (*47*) was used. The integration time step was set to 2 fs, and Na^+ ions were added to neutralize the total charge of the system. Particle mesh Ewald summation with a grid spacing of 1.2 Å was used to calculate long-range electrostatic interactions. After equilibration, the production run was performed in the NPT ensemble at 300 K and 1 atm for 1 μs. Amide order parameters S^2(MD) were back-calculated from MD trajectories using the iRED method with varying lengths of the time-averaging window (*48*). PCA was performed on the backbone dihedral angles of loop residues.

SUPPLEMENTARY MATERIALS

Supplementary material for this article is available at http://advances.sciencemag.org/cgi/content/full/5/8/eaax5560/DC1

Supplementary Materials and Methods

Fig. S1. Simulated dependence of R_2^{free} and ΔR_2 on internal correlation time τ_i and S^2 order parameter.

Fig. S2. Range of validity of Eq. 3 for the extraction of S^2 from ΔR_2.

Fig. S3. Experimental ^{15}N spin relaxation parameters of Im7 in the absence of NPs.

Fig. S4. Experimental ^{15}N spin relaxation parameters of CBD1 in the absence of NPs.

Fig. S5. Comparison between NMR $S^2(\Delta R_2)$ and x-ray B-factors of backbone nitrogen atoms in crystal structures.

Fig. S6. Dependence of ΔR_2 values on SNP concentration.

Fig. S7. Mapping of experimental $S^2(\Delta R_2)$ onto the structural model of Im7 when bound to the DNase domain of colicin E7.

References (*49*–*63*)

REFERENCES AND NOTES

1. J. Cavanagh, W. J. Fairbrother, A. G. Palmer III, M. Rance, N. J. Skelton, *Protein NMR Spectroscopy: Principles and Practice* (Academic Press, ed. 2, 2007).
2. R. Ishima, D. A. Torchia, Protein dynamics from NMR. *Nat. Struct. Mol. Biol.* **7**, 740–743 (2000).
3. A. Mittermaier, L. E. Kay, New tools provide new insights in NMR studies of protein dynamics. *Science* **312**, 224–228 (2006).
4. R. Brüschweiler, New approaches to the dynamic interpretation and prediction of NMR relaxation data from proteins. *Curr. Opin. Struct. Biol.* **13**, 175–183 (2003).
5. C. Redfield, J. Boyd, L. J. Smith, R. A. G. Smith, C. M. Dobson, Loop mobility in a four-helix-bundle protein: Nitrogen-15 NMR relaxation measurements on human interleukin-4. *Biochemistry* **31**, 10431–10437 (1992).
6. R. Brüschweiler, X. Liao, P. E. Wright, Long-range motional restrictions in a multidomain zinc-finger protein from anisotropic tumbling. *Science* **268**, 886–889 (1995).
7. E. Z. Eisenmesser, O. Millet, W. Labeikovsky, D. M. Korzhnev, M. Wolf-Watz, D. A. Bosco, J. J. Skalicky, L. E. Kay, D. Kern, Intrinsic dynamics of an enzyme underlies catalysis. *Nature* **438**, 117–121 (2005).
8. D. D. Boehr, D. McElheny, H. J. Dyson, P. E. Wright, The dynamic energy landscape of dihydrofolate reductase catalysis. *Science* **313**, 1638–1642 (2006).
9. S. K. Whittier, A. C. Hengge, J. P. Loria, Conformational motions regulate phosphoryl transfer in related protein tyrosine phosphatases. *Science* **341**, 899–903 (2013).
10. M. Tollinger, N. R. Skrynnikov, F. A. A. Mulder, J. D. Forman-Kay, L. E. Kay, Slow dynamics in folded and unfolded states of an SH3 domain. *J. Am. Chem. Soc.* **123**, 11341–11352 (2001).
11. R. Schneider, D. Maurin, G. Communie, J. Kragelj, D. F. Hansen, R. W. H. Ruigrok, M. R. Jensen, M. Blackledge, Visualizing the molecular recognition trajectory of an intrinsically disordered protein using multinuclear relaxation dispersion NMR. *J. Am. Chem. Soc.* **137**, 1220–1229 (2015).
12. A. L. Lee, S. A. Kinnear, A. J. Wand, Redistribution and loss of side chain entropy upon formation of a calmodulin–peptide complex. *Nat. Struct. Biol.* **7**, 72–77 (2000).
13. Q. Zhang, X. Sun, E. D. Watt, H. M. Al-Hashimi, Resolving the motional modes that code for RNA adaptation. *Science* **311**, 653–656 (2006).
14. A. G. Palmer III, Chemical exchange in biomacromolecules: Past, present, and future. *J. Magn. Reson.* **241**, 3–17 (2014).
15. J. G. Reddy, S. Pratihar, D. Ban, S. Frischkorn, S. Becker, C. Griesinger, D. Lee, Simultaneous determination of fast and slow dynamics in molecules using extreme CPMG relaxation dispersion experiments. *J. Biomol. NMR* **70**, 1–9 (2018).
16. P. Vallurupalli, G. Bouvignies, L. E. Kay, Studying "invisible" excited protein states in slow exchange with a major state conformation. *J. Am. Chem. Soc.* **134**, 8148–8161 (2012).
17. N. J. Anthis, G. M. Clore, Visualizing transient dark states by NMR spectroscopy. *Q. Rev. Biophys.* **48**, 35–116 (2015).
18. D. M. Heyes, M. J. Nuevo, J. J. Morales, A. C. Branka, Translational and rotational diffusion of model nanocolloidal dispersions studied by molecular dynamics simulations. *J. Phys. Condens. Matter* **10**, 10159–10178 (1998).
19. G. Lipari, A. Szabo, Model-free approach to the interpretation of nuclear magnetic resonance relaxation in macromolecules. 1. Theory and range of validity. *J. Am. Chem. Soc.* **104**, 4546–4559 (1982).
20. G. Papadakos, J. A. Wojdyla, C. Kleanthous, Nuclease colicins and their immunity proteins. *Q. Rev. Biophys.* **45**, 57–103 (2012).
21. A. P. Capaldi, M. C. R. Shastry, C. Kleanthous, H. Roder, S. E. Radford, Ultrarapid mixing experiments reveal that Im7 folds *via* an on-pathway intermediate. *Nat. Struct. Biol.* **8**, 68–72 (2001).
22. S. B.-M. Whittaker, N. J. Clayden, G. R. Moore, NMR characterisation of the relationship between frustration and the excited state of Im7. *J. Mol. Biol.* **414**, 511–529 (2011).
23. C. R. Weber, K. S. Ginsburg, K. D. Philipson, T. R. Shannon, D. M. Bers, Allosteric regulation of Na/Ca exchange current by cytosolic Ca in intact cardiac myocytes. *J. Gen. Physiol.* **117**, 119–131 (2001).
24. D. A. Nicoll, M. R. Sawaya, S. Kwon, D. Cascio, K. D. Philipson, J. Abramson, The crystal structure of the primary Ca^{2+} sensor of the Na^+/Ca^{2+} exchanger reveals a novel Ca^{2+} binding motif. *J. Biol. Chem.* **281**, 21577–21581 (2006).
25. S. M. S. Murshed, P. Estellé, A state of the art review on viscosity of nanofluids. *Renewable Sustainable Energy Rev.* **76**, 1134–1152 (2017).
26. E. Johnson, L. Bruschweiler-Li, S. A. Showalter, G. W. Vuister, F. Zhang, R. Brüschweiler, Structure and dynamics of Ca^{2+}-binding domain 1 of the Na^+/Ca^{2+} exchanger in the presence and in the absence of Ca^{2+}. *J. Mol. Biol.* **377**, 945–955 (2008).
27. A. L. Hansen, L. E. Kay, Quantifying millisecond time-scale exchange in proteins by CPMG relaxation dispersion NMR spectroscopy of side-chain carbonyl groups. *J. Biomol. NMR* **50**, 347–355 (2011).
28. Y. Gu, D.-W. Li, R. Brüschweiler, NMR order parameter determination from long molecular dynamics trajectories for objective comparison with experiment. *J. Chem. Theory Comput.* **10**, 2599–2607 (2014).
29. J. Wang, R. Brüschweiler, 2D entropy of discrete molecular ensembles. *J. Chem. Theory Comput.* **2**, 18–24 (2006).
30. M. Zeeb, M. H. Jacob, T. Schindler, J. Balbach, ^{15}N relaxation study of the cold shock protein CspB at various solvent viscosities. *J. Biomol. NMR* **27**, 221–234 (2003).
31. J. Xu, Y. Xue, N. R. Skrynnikov, Detection of nanosecond time scale side-chain jumps in a protein dissolved in water/glycerol solvent. *J. Biomol. NMR* **45**, 57–72 (2009).
32. S. F. Cousin, P. Kadeřávek, N. Bolik-Coulon, Y. Gu, C. Charlier, L. Carlier, L. Bruschweiler-Li, T. Marquardsen, J.-M. Tyburn, R. Brüschweiler, F. Ferrage, Time-resolved protein side-chain motions unraveled by high-resolution relaxometry and molecular dynamics simulations. *J. Am. Chem. Soc.* **140**, 13456–13465 (2018).

33. M. Assfalg, L. Ragona, K. Pagano, M. D'Onofrio, S. Zanzoni, S. Tomaselli, H. Molinari, The study of transient protein–nanoparticle interactions by solution NMR spectroscopy. *Biochim. Biophys. Acta Proteins Proteom.* **1864**, 102–114 (2016).
34. M. Xie, D.-W. Li, J. Yuan, A. L. Hansen, R. Brüschweiler, Quantitative binding behavior of intrinsically disordered proteins to nanoparticle surfaces at individual residue level. *Chem. Eur. J.* **24**, 16997–17001 (2018).
35. N. G. Housden, C. Kleanthous, Thermodynamic dissection of colicin interactions, in *Methods in Enzymology*, M. L. Johnson, J. M. Holt, G. K. Ackers, Eds. (Academic Press, 2011), vol. 488, chap. 6, pp. 123–145.
36. G. Schreiber, G. Haran, H.-X. Zhou, Fundamental aspects of protein–protein association kinetics. *Chem. Rev.* **109**, 839–860 (2009).
37. M. Akke, R. Brüschweiler, A. G. Palmer III, NMR order parameters and free energy: An analytical approach and its application to cooperative Ca^{2+} binding by calbindin D_{9k}. *J. Am. Chem. Soc.* **115**, 9832–9833 (1993).
38. K. A. Beauchamp, Y.-S. Lin, R. Das, V. S. Pande, Are protein force fields getting better? A systematic benchmark on 524 diverse NMR measurements. *J. Chem. Theory Comput.* **8**, 1409–1414 (2012).
39. A. Bax, A. Grishaev, Weak alignment NMR: A hawk-eyed view of biomolecular structure. *Curr. Opin. Struct. Biol.* **15**, 563–570 (2005).
40. O. F. Lange, N.-A. Lakomek, C. Farès, G. F. Schröder, K. F. A. Walter, S. Becker, J. Meiler, H. Grubmüller, C. Griesinger, B. L. de Groot, Recognition dynamics up to microseconds revealed from an RDC-derived ubiquitin ensemble in solution. *Science* **320**, 1471–1475 (2008).
41. B. Shi, Y. K. Shin, A. A. Hassanali, S. J. Singer, DNA binding to the silica surface. *J. Phys. Chem. B* **119**, 11030–11040 (2015).
42. M. Xie, A. L. Hansen, J. Yuan, R. Brüschweiler, Residue-specific interactions of an intrinsically disordered protein with silica nanoparticles and their quantitative prediction. *J. Phys. Chem. C* **120**, 24463–24468 (2016).
43. N.-A. Lakomek, J. Ying, A. Bax, Measurement of ^{15}N relaxation rates in perdeuterated proteins by TROSY-based methods. *J. Biomol. NMR* **53**, 209–221 (2012).
44. M. Gairí, A. Dyachenko, M. T. González, M. Feliz, M. Pons, E. Giralt, An optimized method for ^{15}N R_1 relaxation rate measurements in non-deuterated proteins. *J. Biomol. NMR* **62**, 209–220 (2015).
45. M. J. Abraham, T. Murtola, R. Schulz, S. Páll, J. C. Smith, B. Hess, E. Lindahl, GROMACS: High performance molecular simulations through multi-level parallelism from laptops to supercomputers. *SoftwareX* **1-2**, 19–25 (2015).
46. D.-W. Li, R. Brüschweiler, NMR-based protein potentials. *Angew. Chem. Int. Ed. Engl.* **49**, 6778–6780 (2010).
47. W. L. Jorgensen, J. Chandrasekhar, J. D. Madura, R. W. Impey, M. L. Klein, Comparison of simple potential functions for simulating liquid water. *J. Chem. Phys.* **79**, 926–935 (1983).
48. J. J. Prompers, R. Brüschweiler, General framework for studying the dynamics of folded and nonfolded proteins by NMR relaxation spectroscopy and MD simulation. *J. Am. Chem. Soc.* **124**, 4522–4534 (2002).
49. S. A. Showalter, L. Bruschweiler-Li, E. Johnson, F. Zhang, R. Brüschweiler, Quantitative lid dynamics of MDM2 reveals differential ligand binding modes of the p53-binding cleft. *J. Am. Chem. Soc.* **130**, 6472–6478 (2008).
50. B. Zhang, M. Xie, L. Bruschweiler-Li, K. Bingol, R. Brüschweiler, Use of charged nanoparticles in NMR-based metabolomics for spectral simplification and improved metabolite identification. *Anal. Chem.* **87**, 7211–7217 (2015).
51. F. A. A. Mulder, R. A. de Graaf, R. Kaptein, R. Boelens, An off-resonance rotating frame relaxation experiment for the investigation of macromolecular dynamics using adiabatic rotations. *J. Magn. Reson.* **131**, 351–357 (1998).
52. A. G. Palmer III, C. D. Kroenke, J. P. Loria, Nuclear magnetic resonance methods for quantifying microsecond-to-millisecond motions in biological macromolecules, in *Methods in Enzymology*, T. L. James, V. Dötsch, U. Schmitz, Eds. (Academic Press, 2001), vol. 339, chap. 10, pp. 204–238.
53. F. Delaglio, S. Grzesiek, G. W. Vuister, G. Zhu, J. Pfeifer, A. Bax, NMRPipe: A multidimensional spectral processing system based on UNIX pipes. *J. Biomol. NMR* **6**, 277–293 (1995).
54. W. Lee, M. Tonelli, J. L. Markley, NMRFAM-SPARKY: Enhanced software for biomolecular NMR spectroscopy. *Bioinformatics* **31**, 1325–1327 (2015).
55. R. K. Wangsness, F. Bloch, The dynamical theory of nuclear induction. *Phys. Rev.* **89**, 728–739 (1953).
56. F. Bloch, Dynamical theory of nuclear induction. II. *Phys. Rev.* **102**, 104–135 (1956).
57. A. G. Redfield, On the theory of relaxation processes. *IBM J. Res. Dev.* **1**, 19–31 (1957).
58. A. Abragam, *The Principles of Nuclear Magnetism* (Clarendon Press, 1961).
59. G. Lipari, A. Szabo, Model-free approach to the interpretation of nuclear magnetic resonance relaxation in macromolecules. 2. Analysis of experimental results. *J. Am. Chem. Soc.* **104**, 4559–4570 (1982).
60. G. M. Clore, A. Szabo, A. Bax, L. E. Kay, P. C. Driscoll, A. M. Gronenborn, Deviations from the simple two-parameter model-free approach to the interpretation of nitrogen-15 nuclear magnetic relaxation of proteins. *J. Am. Chem. Soc.* **112**, 4989–4991 (1990).
61. A. Šali, T. L. Blundell, Comparative protein modelling by satisfaction of spatial restraints. *J. Mol. Biol.* **234**, 779–815 (1993).
62. A. Altis, P. H. Nguyen, R. Hegger, G. Stock, Dihedral angle principal component analysis of molecular dynamics simulations. *J. Chem. Phys.* **126**, 244111 (2007).
63. T.-P. Ko, C.-C. Liao, W.-Y. Ku, K.-F. Chak, H. S. Yuan, The crystal structure of the DNase domain of colicin E7 in complex with its inhibitor Im7 protein. *Structure* **7**, 91–102 (1999).

Acknowledgments: We thank L. E. Kay for providing the plasmid of Im7 and AkzoNobel for the SNPs. **Funding:** This work was supported by the U.S. NSF (grant MCB-1715505 to R.B.). NMR experiments were performed at the CCIC NMR facility at The Ohio State University, and MD simulations were performed at the Ohio Supercomputer Center. **Author contributions:** M.X. prepared NP samples, performed NMR relaxation experiments, and analyzed data. L.Y. performed and analyzed MD simulations and compared them with experimental data. L.B.-L. subcloned Im7, expressed and isotopically labeled Im7 and CBD1, and prepared samples with NPs and for assignments. X.X. performed resonance assignments of Im7. A.L.H. performed NMR relaxation and assignment experiments, confirmed CBD1 assignments, and analyzed data. R.B. conceived the project, developed the theory, interpreted data, and wrote the manuscript with input from M.X., L.Y., and A.L.H. **Competing interests:** The corresponding author filed an invention disclosure related to this work. The authors declare no other competing interests. **Data and materials availability:** All data needed to evaluate the conclusions in the paper are present in the paper and/or the Supplementary Materials. Additional data related to this paper may be requested from the authors.

Submitted 2 April 2019
Accepted 9 July 2019
Published 14 August 2019
10.1126/sciadv.aax5560

Citation: M. Xie, L. Yu, L. Bruschweiler-Li, X. Xiang, A. L. Hansen, R. Brüschweiler, Functional protein dynamics on uncharted time scales detected by nanoparticle-assisted NMR spin relaxation. *Sci. Adv.* **5**, eaax5560 (2019).